Cell, Vol. 103, 467–479, October 27, 2000, Copyright ©2000 by Cell Press

Insights into the Molecular Basis of Leukocyte Tethering and Rolling Revealed by Structures of P- and E-Selectin Bound to SLe^X and PSGL-1

William S. Somers, Jin Tang, Gray D. Shaw, and Raymond T. Camphausen*
Genetics Institute
Wyeth Research
87 CambridgePark Drive
Cambridge, Massachusetts 02140

Summary

P-, E- and L-selectin constitute a family of cell adhesion receptors that mediate the initial tethering and rolling of leukocytes on inflamed endothelium as a prelude to their firm attachment and extravasation into tissues. The selectins bind weakly to sialyl Lewis^x (SLe^x)-like glycans, but with high-affinity to specific glycoprotein counterreceptors, including PSGL-1. Here, we report crystal structures of human P- and E-selectin constructs containing the lectin and EGF (LE) domains co-complexed with SLe^x. We also present the crystal structure of P-selectin LE co-complexed with the N-terminal domain of human PSGL-1 modified by both tyrosine sulfation and SLe^x. These structures reveal differences in how E- and P-selectin bind SLe^x and the molecular basis of the high-affinity interaction between P-selectin and PSGL-1.

Introduction

The selectins are a family of cell-surface glycoproteins responsible for early adhesion events in the recruitment of leukocytes into sites of inflammation and their emigration into lymphatic tissues (Kansas, 1996; Vestweber and Blanks, 1999). As part of a multistep process (Springer, 1994), selectins promote the initial attachment (tethering) and subsequent movement (rolling) of leukocytes over vessel walls where they become activated as a consequence of exposure to locally produced chemokines. Firm adhesion of the leukocytes mediated by integrins precedes their extravasation into the underlying tissue. P-selectin (CD62P) and E-selectin (CD62E) are induced on the surface of vascular endothelium in response to inflammatory stimuli but with different expression kinetics. P-selectin, which is also presented by activated platelets, is translocated within minutes from intracellular stores and promotes the immediate attachment and rapid rolling of leukocytes over vascular surfaces. In contrast, E-selectin is transcriptionally regulated appearing on the activated endothelium within hours and produces slower rolling of leukocytes likely important for their subsequent firm attachment. L-selectin (CD62L) is expressed constitutively on leukocytes and may function to amplify inflammatory processes by promoting leukocyte-leukocyte and leukocyte-endothelium interactions. In addition to its role in inflammation, L-selectin mediates the attachment of lymphocytes to specialized high endothelial venules (HEV) in the course of their migration from the blood to lymphoid tissues.

Cell attachment and rolling under the influence of hydrodynamic shear stresses within the vasculature require that the selectins possess unique biophysical and molecular properties. The selectins exhibit rapid binding kinetics (Alon et al., 1995; Alon et al., 1997), and this may account for their ability to mediate transient tethers and to produce a dynamic contact zone that moves along the vascular endothelium during rolling. Mechanical properties that distinguish this class of adhesion receptors from others that bind with similar kinetics may also play a role in function (Alon et al., 1995; Chen et al., 1997; Puri et al., 1998). Structurally similar, the selectins consist of an N-terminal, calcium-dependent lectin domain (Drickamer, 1988), an epidermal growth factor-like (EGF) domain, variable numbers of complement regulatory-like units, a transmembrane domain, and an intracellular region. The primary basis of adhesion is relatively weak, calcium-dependent interactions between the lectin domain and glycan ligands on apposing cells. Other selectin domains, particularly the EGF domain, are reported to modulate function, but the nature of their contributions is uncertain (Kansas, 1996). Although a number of small and large molecular weight glycans bind to the selectins (Varki, 1994), an epitope displayed by the sialyl Lewis^x (SLe^x, NeuNAcα2,3Galβ1,4[Fucα1, 3]GlcNAc) tetrasaccharide and related structures is a physiologically relevant recognition component common to all three members of the family (Foxall et al., 1992).

Structurally diverse glycoprotein counterreceptors, including GlyCAM-1, CD34, ESL-1, and PSGL-1 bind the selectins with apparent high-affinity (Kansas, 1996; Vestweber and Blanks, 1999), but their physiological relevancy and the basis of their increased affinity relative to SLe^x-type glycans are in most cases uncertain (Varki, 1994; Varki, 1997). PSGL-1, a mucin-like homodimeric glycoprotein expressed by virtually all subsets of leukocytes and recognized by all three selectins (Sako et al. 1993; McEver and Cummings, 1997; Yang et al., 1999a) is perhaps the best characterized of these at a structure-function level. High-affinity P-selectin binding requires both a SLe^x-containing O-glycan and one or more tyrosine sulfate residues within the anionic N terminus of the PSGL-1 polypeptide (Pouyani and Seed, 1995; Sako et al., 1995; Wilkins et al., 1995). Both tyrosine sulfation and SLe^x modification of this region of PSGL-1 are required for P-selectin function under the influence of shear flow (Goetz et al., 1997; Ramachandran et al., 1999). Furthermore, PSGL-1-deficient mice exhibit severe reductions in P-selectin-mediated cell rolling and early neutrophil recruitment, demonstrating the importance of this counterreceptor for in vivo function (Yang et al., 1999b). L-selectin also recognizes the N-terminal region of PSGL-1 and has similar, if not identical, binding requirements of P-selectin; the L-selectin/PSGL-1 interaction may be important for the capture of free-flowing neutrophils by adherent neutrophils (McEver and Cummings, 1997; Yang et al., 1999a). Although PSGL-1 supports E-selectin binding in a tyrosine sulfate-indepen-

*To whom correspondence should be addressed (e-mail: rcamphausen@genetics.com).

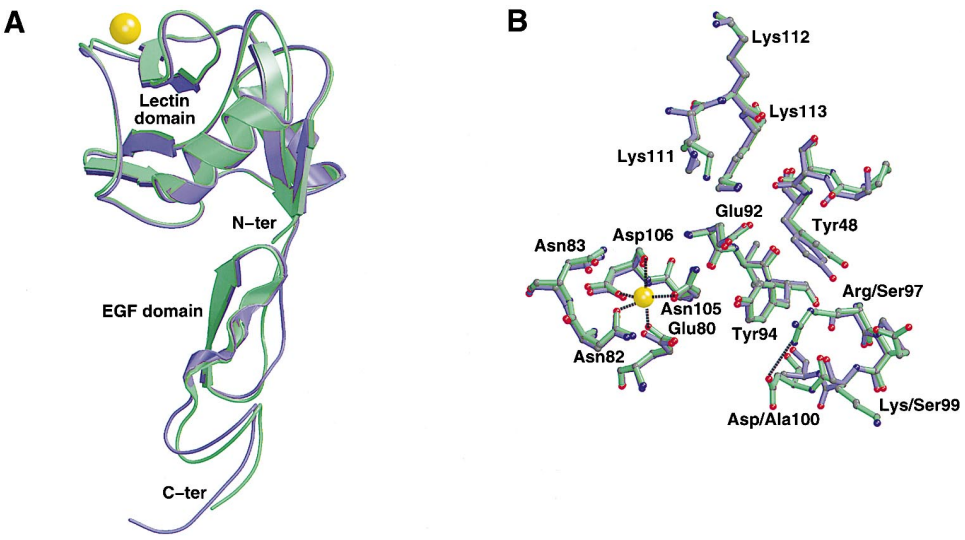

Figure 1. Comparison of P-LE to the Structure of E-LE (Graves et al., 1994)

(A) Ribbon representation of the optimal superposition of P-LE and the previously described E-LE structure showing overall similarity. P-LE is in blue and E-LE is in green. The bound calcium ions in the two structures are precisely superimposed and are represented as a single yellow sphere.

(B) A ball and stick representation of the superposition of P-LE and E-LE residues in the vicinity of the SLe^x binding site. The coloring scheme and superposition of calcium ions is identical to that in Figure 1A. For clarity, only interactions with the bound calcium in E-LE are shown as dashed lines. The stabilizing hydrogen bond between Arg97 and Asp100 in E-selectin is also shown as a dashed line. For residues that differ between E- and P-selectin, E-selectin residues are listed first. All structure figures were produced with MOLSCRIPT (Kraulis, 1991) and RASTER3D (Merrit and Murphy, 1994) except where noted.

dent manner (Pouyani and Seed, 1995; Sako et al., 1995), this interaction is not required for cell attachment and rolling in vivo (Yang et al., 1999b). Additional SLe^x-modified glycoconjugates support binding (Kansas, 1996) suggesting that E-selectin recognition of PSGL-1 is dependent upon the presentation of SLe^x-type glycans alone and not on polypeptide-encoded determinants.

The molecular bases of selectin interactions are poorly characterized. Although the crystal structure of an E-selectin lectin/EGF construct has been solved (Graves et al., 1994), structures of other selectins and of selectins complexed with SLe^x-type glycans and counterreceptors have not been reported. In an effort to increase our understanding of selectin interactions, we produced an X-ray crystal structure of the lectin/EGF (LE) domains of human P-selectin (P-LE). We introduced the SLe^x tetrasaccharide into these crystals, as well as into crystals of a human E-selectin construct (E-LE) that we generated in similar fashion. We also obtained a crystal structure of P-LE complexed with the N-terminal domain of human PSGL-1 that is posttranslationally modified by tyrosine sulfation and SLe^x. These structures reveal the molecular interactions of P- and E-selectin with this common ligand and counterreceptor and offer insight into the nature of the binding interactions underlying selectin-mediated leukocyte tethering and rolling.

Results and Discussion

X-Ray Crystal Structure of the P-Selectin LE Construct

We expressed a human P-selectin construct in CHO cells that is structurally similar to the E-selectin lectin/EGF (E-LE) construct crystallized earlier (Graves et al., 1994). P-selectin containing only these two domains binds to PSGL-1 with high-affinity (Mehta et al., 1997). P-LE crystals have four copies of P-LE in the asymmetric unit. The structure was solved at 2.4 Å resolution and refined to an R-factor of 21.3% and an R_{free} of 25.2% (Table 1). The P-LE crystal structure adopts an overall conformation similar to that of the previously described E-LE structure (Graves et al., 1994) consistent with the ~60% sequence identity between the selectins in these domains (Figure 1A). This results in a r.m.s. difference of only 0.7 Å for their Cα backbones. The lectin and EGF domains of P-LE interact via a small interface making the similarity with the E-LE construct even more striking since this interdomain relationship is also maintained (Figure 1A). The movement of several loops in the EGF domain and a small movement of the interdomain angle within P-LE are responsible for many of the minor differences between the two structures. The interdomain angle also varies slightly between different copies of P-LE in the crystal. This may reflect flexibility in this region of the molecule or may be an effect of crystal packing forces.

The SLe^x binding site is highly conserved between the P-LE and E-LE structures. The common feature of this site, and the basis for the metal-dependency of selectin function, is the coordination of a calcium ion by the side chains of Glu80, Asn82, Asn105, and Asp106 and the backbone carbonyl of Asp106 (Figure 1B). The binding sites do have differences, however, in one area defined by the substitution of Arg97-Glu98-Lys99-Asp100 in E-selectin with Ser97-Pro98-Ser99-Ala100 in P-selectin (Figure 1B). In E-LE, Arg97 is stabilized by a hydrogen bond to Asp100 and stacks on Tyr94, thereby

Table 1. Data Collection, Phasing and Refinement Statistics

Structure	P-LE	P-LE/SLe^x	E-LE/SLe^x	P-LE/SGP-3	P-LE/SGP-3/Hg
Data Collection					
Resolution Range (Å)	15.0–2.4 (2.49–2.4)	14.0–3.4 (3.46–3.4)	15.0–1.5 (1.55–1.5)	15.0–1.9 (1.97–1.90)	14.0–3.5 (3.62–3.50)
R_{sym}[a] (%)	5.2 (22.5)	7.2 (32.2)	4.1 (22.0)	5.8 (27.4)	5.5 (7.5)
% Completeness	95.8 (74.2)	97.8 (100.0)	92.4 (62.0)	98.5 (96.6)	97.0 (94.0)
Total Observations	240,361	44,334	260,283	207,998	33,998
Unique Reflections	32,570	11,667	29,493	44,923	7,240
$<I/\sigma(I)>$	35.7 (6.6)	29.0 (5.4)	47.6 (4.4)	25.5 (3.7)	27.4 (18.2)
Phasing[b]					
Phasing Power					
Centrics—Isomorphous					0.94
Acentrics—Isomorphous					1.17
Acentrics—Anomalous					1.47
Isomorphous Difference on I (%)					32.2
Number of Sites					1
FOM (Centric/Acentric)					0.312/0.428
Model Refinement					
Resolution (Å)	14.0–2.4	14.0–3.4	14.0–1.5	14.0–1.9	
R-factor (%)	21.3	22.7	19.6	20.4	
R_{free}[c] (%)	25.2	32.2	21.7	23.5	
<B value> (Å^2)	48.8	54.1	19.9	42.0	
RMS deviations from ideal geometry:					
Bonds (Å)	0.010	0.011	0.009	0.010	
Angles (°)	1.46	1.53	1.42	1.54	
RMS difference in main chain bonded B values (Å^2)	3.5	3.5	1.83	3.1	

[a] $R_{sym} = \Sigma|I_h - <I_h>|/\Sigma I_h$ where $<I_h>$ is the average intensity over symmetry equivalents. Numbers in parenthesis refer to statistics for the final resolution shell.

[b] Phasing statistics as reported by SHARP.

[c] R_{free} represents the R-factor for a randomly selected set of reflections representing 5% of the data not used in refinement.

presenting a positively charged surface in this region (Figure 1B). In contrast, both of these positions are uncharged, non-interacting residues in P-LE. Lys99 in E-LE points away from the binding site, whereas Ser99 in P-LE is directed inward (Figure 1B).

Crystal Structures of P- and E-Selectin LE Domains Complexed with SLe^X

P-selectin-mediated, but not E-selectin-mediated, leukocyte rolling and recruitment are dramatically affected in mice genetically deficient in PSGL-1 (Yang et al., 1999b). This suggests that, in vivo, E-selectin effectively utilizes other SLe^X-modified glycoconjugates on leukocytes, whereas P-selectin does not. Although the role of avidity due to differences in selectin expression is uncertain, differential affinities of E- and P-selectin for leukocyte ligands and counterreceptors are likely important factors in this distinction. P-selectin binds SLe^X-modified PSGL-1 with nanomolar binding affinity (Croce et al., 1998; Mehta et al., 1998). This is significantly higher in affinity than the E-selectin/PSGL-1 interaction (Moore et al., 1994). In contrast, P-selectin binds the SLe^X ligand with a K_D of 7.8 mM, approximately 10-fold lower affinity than the E-selectin/SLe^X interaction (Poppe et al., 1997). To explore the structural basis for the different affinities for SLe^X, we soaked this ligand into preformed crystals of P-LE and into crystals of a human E-selectin construct (E-LE) that was prepared similarly to P-LE. The P-LE/SLe^X diffraction data extend to 3.4 Å (Table 1). Three copies of P-LE within the asymmetric unit contain bound SLe^X; the binding site of the fourth copy is partially occluded by crystal contacts. Our E-LE crystallized under conditions similar to those employed for the earlier construct (B. Graves, personal communication) with one copy in the crystallographic asymmetric unit; it is essentially identical to the earlier structure (Graves et al., 1994). E-LE crystals were soaked with SLe^X using conditions that gave diffraction data extending to 1.5 Å and clear electron density for the bound ligand (Table 1).

SLe^X binds to P- and E-LE, using essentially the same site and with similar conformation of the tetrasaccharide (Figure 2A). There are differences that account for the altered binding affinity for this ligand, however. The structures of the SLe^X complexes reveal that the interactions are almost entirely electrostatic in nature, and the total buried surface area is small (549 Å^2 in E-LE and 501 Å^2 in P-LE) when compared to the size of the free ligand. In both structures, the selectin-bound calcium ion is ligated by the 3- and 4-hydroxyl groups of the Fuc residue within SLe^X (Figure 2B). This arrangement is in sharp contrast to proposed models of selectin/SLe^X interactions (Bertozzi, 1995) that predict Fuc ligation to calcium via the 2- and 3-hydroxyl groups based on the structure of the homologous rat mannose binding protein (MBP) complexed with oligomannose (Weis et al., 1992). The Fuc hydroxyl groups must provide a large amount of the SLe^X binding energy; they not only coordinate the bound calcium but also form hydrogen bonds

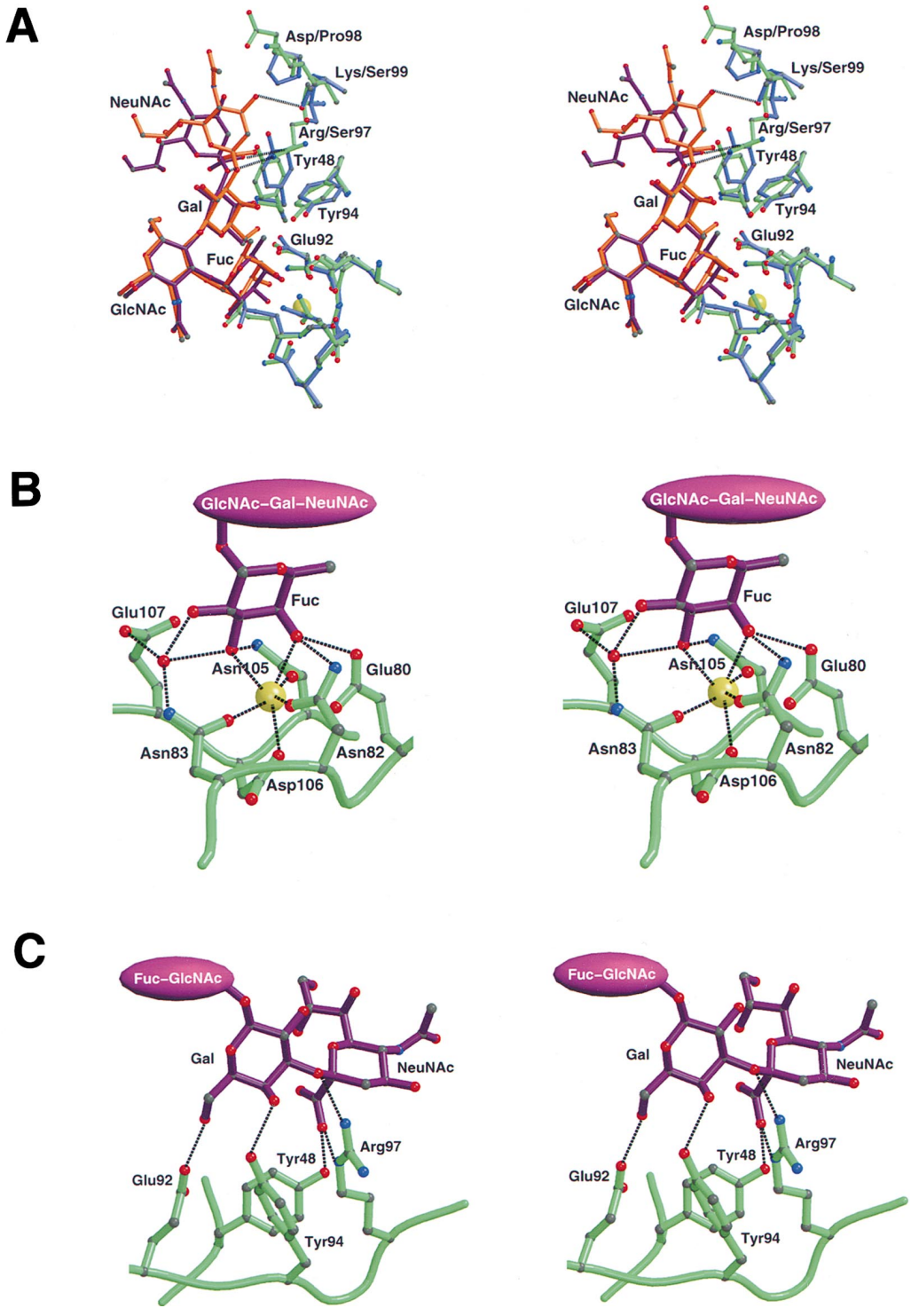

Figure 2. P-LE/SLe^X and E-LE/SLe^X Interactions

(A) A ball and stick stereo view of the superposition of SLe^X bound to P-LE and E-LE showing the similarity in binding orientation. P-LE residues are in blue, E-LE residues are in green, and the precisely superimposed calcium ions are shown as a single yellow sphere. SLe^X bound to P-LE is in orange and SLe^X bound to E-LE is in purple. Dashed lines represent hydrogen bonds distinguishing NeuNAc binding by P-LE (Ser99) from E-LE (Arg97). For clarity, residues involved in calcium ligation and hydrogen bond formation to Fuc in SLe^X are not labeled. These are presented in Figure 2B.

(B) Stereo view of SLe^X bound to E-LE focusing on the Fuc interaction. E-LE is shown in green, SLe^X residues are shown in purple, and the calcium ion is shown as a yellow sphere. A bound water molecule is shown as a red sphere. Dashed lines represent calcium ligation and hydrogen bonds. These interactions are identical in P-LE/SLe^X except where noted in the text. For clarity, calcium coordination bonds for the side chain of Glu80 and the backbone carbonyl of Asp106 are not shown (refer to Figure 1B).

(C) Stereo view of SLe^X bound to E-LE focusing on the Gal and NeuNAc interactions. Refer to Figure 2B for figure descriptions. P-LE binds these residues in similar fashion except for differences noted in the text and Figure 2A.

with selectin residues that are also involved in calcium coordination (Figure 2B). The Fuc 4-hydroxyl group of SLe^X replaces precisely a calcium-ligated water molecule observed in the unliganded structures and hydrogen bonds to Asn82 and Glu80 (Figure 2B). The Fuc 3-hydroxyl group displaces another calcium-coordinated water molecule, although its final position is now one Å closer to Asn105, to which it hydrogen bonds. In the E-LE/SLe^X complex, Asn83 rotates its *X*2 torsion angle to 59°, so that it now hydrogen bonds a water molecule, that in turn hydrogen bonds to the Fuc 2- and 3-hydroxyl groups and Glu107 (Figure 2B). This rotation also allows the Asn83 side chain to coordinate the calcium. Asn83 is not seen to move and form these productive interactions in the P-LE/SLe^X complex.

In both P- and E-LE complexes, the SLe^X Gal residue hydrogen bonds to Tyr94 and Glu92, and the carboxylate group of NeuNAc hydrogen bonds to Tyr48 (Figure 2C). The NeuNAc residue makes additional contacts, however, in a selectin-specific manner, owing to the sequence differences described above. In P-LE, the 4-hydroxyl group of NeuNAc hydrogen bonds to Ser99 (Figure 2A), and the C-4 of the NeuNAc ring packs against Pro98. A more extensive set of interactions is observed within the E-LE complex facilitated by a change in conformation of this sugar residue. The positioning of NeuNAc within the P-LE/SLe^X complex would make unfavorable contacts with Arg99 in E-LE, and so moves further back to allow for better interactions (Figures 2A). In this arrangement, Arg97 hydrogen bonds to the glycosidic oxygen and the carboxylate group of NeuNAc (Figure 2C). These differences, combined with differences in Fuc binding, appear to be the structural basis for the higher affinity E-selectin/SLe^X interaction.

Generation of a Functional PSGL-1 N Terminus for X-Ray Crystallography

We next sought a crystal structure of P-LE complexed with PSGL-1 to elucidate the structural basis of the high-affinity interaction, but anticipated that the membrane-bound form, or large, extracellular constructs of PSGL-1, would prove too heterogeneous for co-crystallization. Therefore, we utilized a highly-truncated Fc construct of human PSGL-1 (19.Fc) that supports high-affinity binding to P-selectin (Sako et al., 1995). This construct encodes the 19 N-terminal amino acids of mature PSGL-1, including three potential Tyr sulfate residues and a SLe^X-modified glycan localized to Thr16. With the specific intention of producing monomeric versions of PSGL-1, 19.Fc was modified to include an enterokinase (EK) cleavage sequence located between the PSGL-1 and Fc sequences (termed 19ek.Fc) (Goetz et al., 1997). Purified 19ek.Fc was digested with EK and the resultant PSGL-1 N-termini (termed 19ek peptides) were resolved by anion-exchange HPLC (Figure 3A). The major 19ek peptide is the sulfoglycopeptide (termed SGP-3) shown in Figure 3A, inset. The PSGL-1 portion of SGP-3 is posttranslationally modified by sulfate on all three tyrosine residues and by a SLe^X-capped O-glycan also found in PSGL-1 isolated from HL-60 cells (Wilkins et al., 1996). SGP-3 is structurally similar to a PSGL-1 glycosulfopeptide produced by in vitro synthesis that binds to P-selectin with high-affinity (Leppanen et al., 1999). SGP-1 and SGP-2 (Figure 3A) are forms of SGP-3 containing one and two tyrosine sulfates, respectively. Also resolved by chromatography (Figure 3A) are versions of SGP-3 containing no tyrosine sulfates (glycopeptide-1, GP-1) or containing no carbohydrate (sulfopeptide-1, SP-1).

We determined the binding affinities of P-LE to the individual 19ek peptides by using surface plasmon resonance (BIAcore) technology. For comparison, we evaluated the affinity of P-LE to a soluble, recombinant form of PSGL-1 (sPSGL) (Croce et al., 1998) comprised of the entire dimeric, extracellular domain. Consistent with earlier studies (Mehta et al., 1998), P-LE binds immobilized sPSGL and 19ek peptides with rapid kinetics (Figure 3B); these interactions are specific based upon control experiments using EDTA and neutralizing Mabs (not shown), and SGP-3 as a soluble inhibitor (Figure 3B). The highest affinity interaction observed for the individual 19ek peptides was to SGP-3 with a K_D of 778 nM, which is essentially identical to the P-LE/sPSGL interaction (Figure 3C). This argues that SGP-3 functionally mimics the full-length extracellular PSGL-1 construct and that the N-terminal region of PSGL-1 present in the shorter, monomeric construct constitutes the entire recognition region for P-LE. P-LE binds with slightly lower affinity to the mono (SGP-1) and disulfated (SGP-2) forms of SGP-3 (Figure 3C), but these differences may be an artifact of the heterogeneity of these species. SGP-1 and SGP-2 are pools comprised of different permutations of sulfated Tyr5 (Tys5), Tys7 and/or Tys10 in unknown relative quantity (data not shown). SGP-2, for example, likely consists of three isoforms: Tys5/Tys7, Tys5/Tys10, and Tys7/Tys10. Therefore, the small differences in P-LE binding affinity may reflect preferential recognition of an isoform that contains sulfate at a specific Tyr position(s), but this is masked by slightly lower affinity interactions with other isoforms. The P-LE binding affinities to versions of SGP-3 containing only the SLe^X glycan (GP-1) or three sulfotyrosines (SP-1) are lower relative to species containing both types of modifications (Figure 3C), but are considerably greater than to a synthetic, unmodified 19ek peptide (not shown). The affinity of the P-LE/GP-1 interaction, however, is significantly greater than the P-selectin/SLe^X interaction (Poppe et al., 1997), suggesting that the PSGL-1 polypeptide contributes to binding in the absence of the sulfotyrosine modification.

X-Ray Crystal Structure of P-LE Bound to the PSGL-1 N-Terminal Peptide

SGP-3 was selected for co-crystallization with P-LE owing to its highest binding affinity and structural homogeneity. The P-LE/SGP-3 complex was solved at 1.9 Å and refined to an R-factor of 20.4% and a R_{free} of 23.5% (Table 1). Of the 28 amino acids within SGP-3, Glu6 through Pro18, including Tys7 and Tys10 are visible (Figure 4). Disordered and absent from the structure are polypeptide residues one through five, including Tys5, and residues 19–28 containing the enterokinase-linker region. All residues of the SLe^X-modified O-glycan at Thr16 are observable, except for the NeuNAc(α2,3)-linked to the Gal(β1,3)GalNAc branch (Figure 3A, inset). This residue does not appear to be required for high-affinity P-selectin binding (Leppanen et al., 1999).

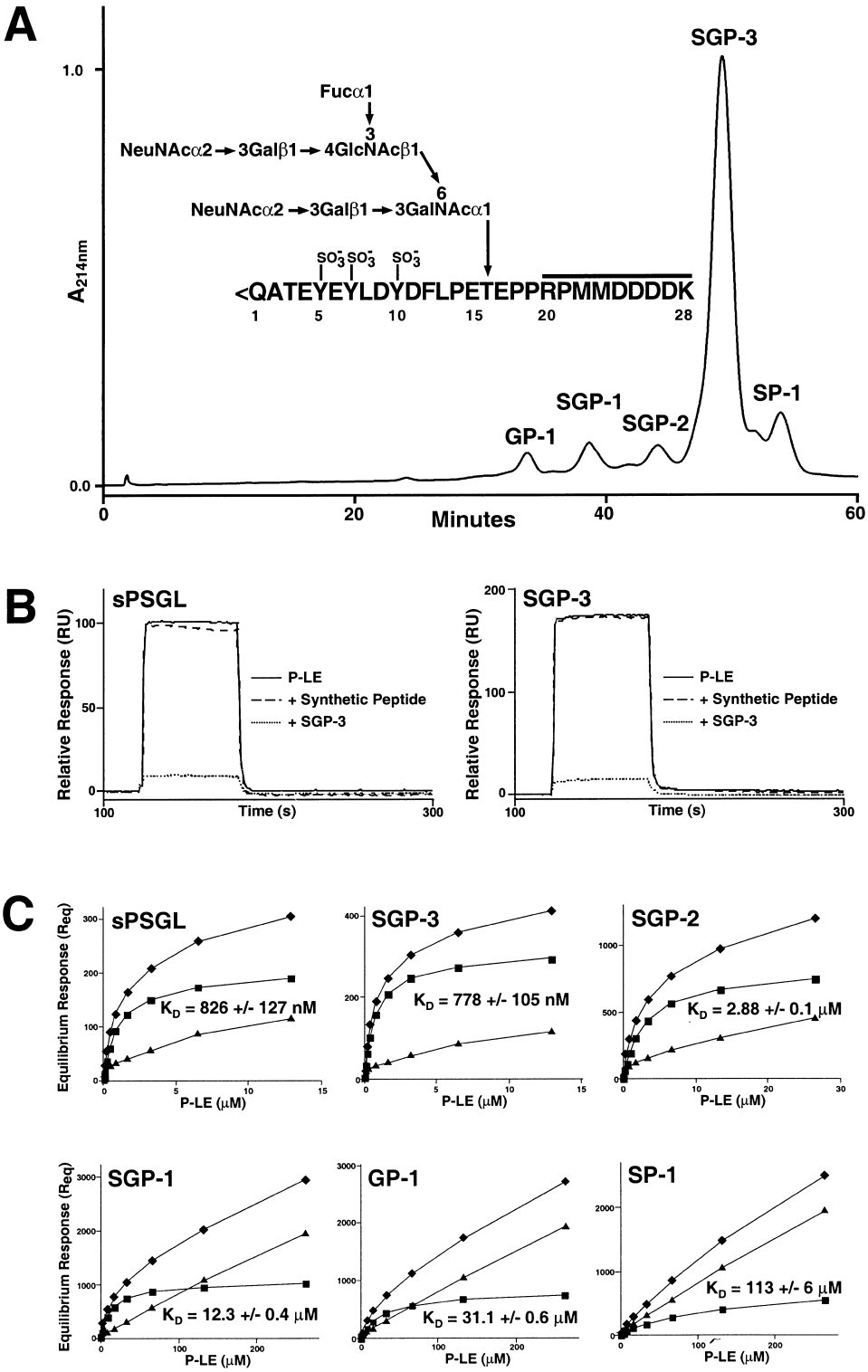

Figure 3. Resolution and BIAcore Affinity Analysis of the PSGL-1 19ek Peptides

(A) Profile of the PSGL-1 19ek peptides resolved by anion-exchange chromatography. See text for definition of peak labels. Inset. Structure of the major PSGL-1 19ek peptide SGP-3. <Q denotes cyclization of the N-terminal Gln residue to pyroglutamate and SO_3 represents sulfation of Tyr residues. The over line in the numbered peptide sequence indicates residues of non-PSGL-1 origin that includes the EK sequence. The numbering of PSGL-1 residues here and in the text is based upon assigning the N terminus of mature PSGL-1 as residue one consistent with our earlier study (Sako et al., 1995).

(B) Representative BIAcore sensorgrams of solution-phase P-LE binding to immobilized PSGL-1 constructs. P-LE (at 800 nM concentration) was injected over sPSGL (left) and SGP-3 (right). Binding signals of P-LE injected other less modified forms of SGP-3 (not shown) were essentially identical to these results with regards to binding kinetics. P-LE binding to sPSGL, and SGP-3 was inhibited by co-injection with

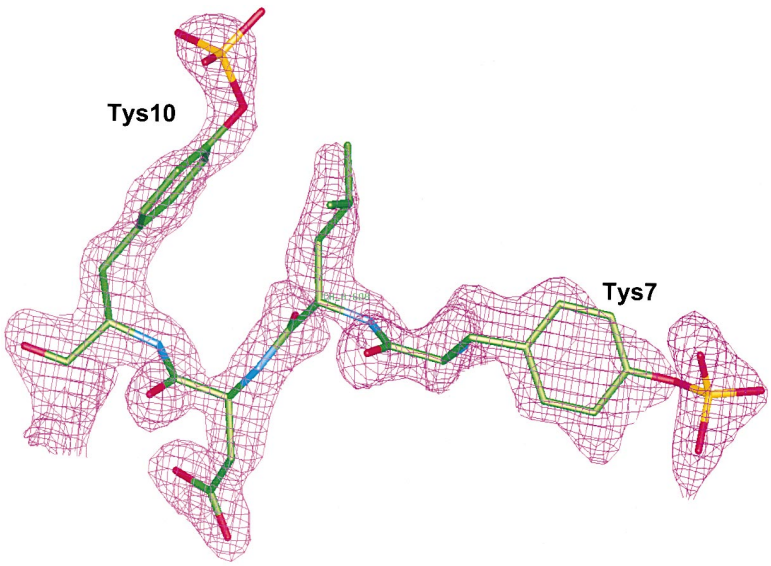

Figure 4. Electron Density of P-LE Bound SGP-3 Residues Tys7 to Tys10

The stick model is from the final refined coordinates of the P-LE/SGP-3 complex. The maximum entropy map was calculated using BUSTER (Bricogne, 1993) including phases derived from P-LE only and the mercury heavy atom derivative. This figure was produced with QUANTA.

Two different views of the P-LE/SGP-3 complex are presented in Figures 5 and 6. SGP-3 binds with 1:1 stoichiometry to the P-LE lectin domain, with a large epitope that excludes 1641 Å^2 from solvent and includes the SLe^X binding site described for the P-LE/SLe^X complex (Figure 5). Despite the fact that SGP-3 is unstructured in solution, as determined by NMR studies (D. Tsao, unpublished observations), and is likely extended (Li et al., 1996), the bound conformation exhibits a hairpin-like structure (Figure 5). The most N-terminal residue of SGP-3 in contact with the protein is Tys7, followed by three residues in an extended conformation (Figure 5). Residues Tys10 to Leu13 form a turn that alters the direction of the peptide, and the remaining residues run to Pro18 in a linear fashion. The anionic, sulfotyrosine-containing portion of the SGP-3 polypeptide binds the P-LE surface in a region of positive electrostatic potential (Figure 5); this region may also support the binding of a number of inhibitory anionic glycoconjugates, including heparin sulfate, fucoidan, and sulfatides (Varki, 1994). In contrast, the SLe^X component of SGP-3 interacts with P-LE in an area of neutral and negative electrostatic potential (Figure 5). The P-LE/SGP-3 complex suggests that individual monomers within dimeric PSGL-1 provide a complete set of P-selectin binding determinants, a result consistent with recent experiments demonstrating that dimerization of PSGL-1 is not required for in vitro function (Epperson et al., 2000). PSGL-1 dimerization may be important in vivo, however; individual monomers of the PSGL-1 homodimer may engage two different P-selectin molecules, in rapid succession and in highly localized fashion, thereby increasing the efficiency of leukocyte tethering and rolling. Also apparent from examination of the P-LE/SGP-3 complex is that the binding of SGP-3 occurs on a face of P-LE essentially opposite the lectin-EGF domain interface (Figure 6A). This argues that the EGF domain of P-selectin does not participate in direct binding to PSGL-1, but it does not exclude an indirect role in function (see below).

The interactions between P-LE and the SGP-3 polypeptide are a combination of electrostatic and hydrophobic contacts. Tys7 appears to be an important component of the high-affinity interaction of PSGL-1 with P-selectin. All three oxygen atoms of the Tys7 sulfate group hydrogen bond, either directly or via a water molecule, to P-LE residues (Figure 6B). Tys7 also makes a backbone-backbone hydrogen bond with the amide nitrogen of Lys112 (Figure 6B) and, through the aromatic ring, several non-polar interactions with the side chains of Ser47 and Lys113 (not shown). This extensive network of hydrogen and non-polar bonds is reminiscent of Tys63 in hirugen complexed with α-thrombin (Skrzypczak-Jankun et al., 1991). SGP-3 residues Leu8 and Leu13 pack against one another and lie against the hydrophobic surface of P-LE formed by His108 and Lys111; these interactions must help stabilize the compact tertiary structure of the peptide. The aromatic ring of the Tys10 side chain of SGP-3 packs against these two leucine residues and orients the sulfate moiety so that it hydrogen bonds to Arg85. Pro14 of SGP-3 packs

solution-phase SGP-3 (dotted line) but not by a synthetic peptide containing no tyrosine sulfation or glycosylation (dashed line), both at 20 μM concentration. All curves reflect specific binding produced by subtracting non-specific binding from total binding.

(C) Binding affinity determinations of solution-phase P-LE reacted with immobilized sPSGL and purified 19ek peptides by BIAcore analysis. First row, left-to-right: sPSGL, SGP-3 and SGP-2. Second row, left-to-right: SGP-1, GP-1 and SP-1. P-LE at the indicated concentrations was reacted with immobilized ligands (to determine the total binding signal) and with control cells containing no ligand (to determine non-specific binding). The equilibrium responses (Req) at each concentration of P-LE are shown. At each P-LE concentration tested, specific binding signals (squares) were determined by subtracting non-specific responses (triangles) from total binding signals (diamonds). K_Ds and standard deviations were determined by line-fitting of specific binding curves using BIAevaluation software (BIAcore) and are the products of three to ten separate experiments. K_D determinations using line-fitting agreed well with values determined by linear regression analysis of Scatchard plots (not shown).

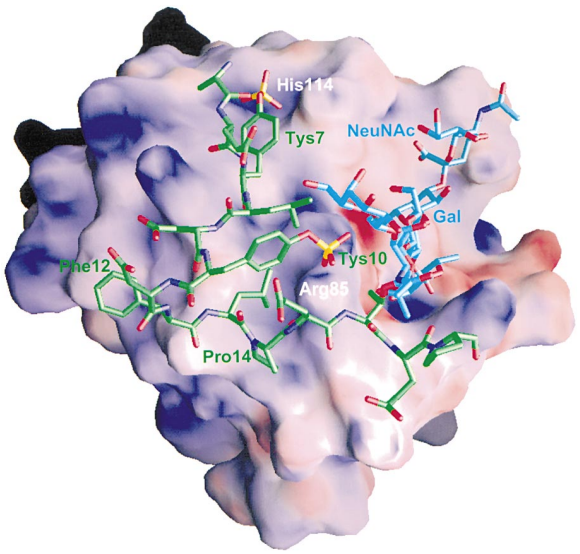

Figure 5. Electrostatic Potential Surface Representation of P-LE with Bound SGP-3

The peptide portion of SGP-3 is shown in green (sulfur is shown as a yellow atom) and the carbohydrate portion in blue. Selected P-LE residues important for the interaction with SGP-3 are labeled in white. For the purpose of orientation, selected SGP-3 residues are labeled in green and in blue. The figure was made with GRASP (Nicholls et al., 1991) and the surface colored with DELPHI (Honig and Nicholls, 1995). Regions with electrostatic potential less than −41 kT are in red and those greater than +55 kT are in blue.

against His108 and also hydrogen bonds to Arg85. The interactions mediated by Arg85 appear to be important determinants for recognition of the PSGL-1 polypeptide, based upon these results and those of an earlier study exploring the role of this specific residue (Bajorath et al., 1994). Despite the fact that strontium was employed for crystallography, interactions between the SLe^X component of SGP-3 and P-LE largely reproduce those observed for the P-LE/SLe^X complex, consistent with the ability of this metal to substitute for calcium (Asa et al., 1992). There do not appear to be direct binding contributions by glycan residues other than those associated with SLe^X.

The binding interactions mediated by Tys7 and Tys10 within the P-LE/SGP-3 complex are consistent with mutagenesis studies demonstrating a preferential role for these PSGL-1 residues for P-selectin-mediated cell rolling under shear flow (Ramachandran et al., 1999). In our structure, however, we do not observe electron density for the third tyrosine sulfate residue in PSGL-1, Tys5, and there are no obvious reasons (e.g., steric exclusion due to crystal contacts) that might account for its absence. This lack of interaction appears to be inconsistent with the observation that sulfation at Tyr5 alone may support P-selectin-mediated cell rolling, albeit less efficiently than PSGL-1 mutants that are presumably monosulfated at Tyr10 or Tyr7 (Ramachandran et al., 1999). In addition, this structure information apparently conflicts with our K_D determinations suggesting that trisulfated SGP-3 interacts to a greater degree with P-LE as compared to disulfated SGP-2. This latter result does not necessarily imply that three Tys binding sites exist within P-LE, however; the Tys7/Tys10 isoform of SGP-2 may bind with comparable affinity to SGP-3, but this is masked by slightly lower affinity interactions with the Tys5/Tys10 and Tys5/Tys7 isoforms. A possible explanation for these inconsistencies is that numerous conformations of the PSGL-1 N terminus bind to P-selectin, the highest affinity of which is revealed by the P-LE/SGP-3 complex. As noted above, PSGL-1 is an extended molecule that, in solution, is likely to be highly flexible. PSGL-1 may bind initially to P-selectin via single, weak interactions using SLe^X or any one of the three Tys residues (Tys5, Tys7, or Tys10) docked into either of the two defined sulfotyrosine binding sites. Flexibility of the PSGL-1 N terminus could then allow formation of complementary interactions that strengthens overall binding to P-selectin. A threshold level of affinity required for effective leukocyte tethering and rolling may be obtained by a variety of single or combinations of two sulfotyrosine residues docked into the defined binding sites in tandem with the SLe^X interaction.

Compared to both unliganded P-LE and the P-LE/SLe^X complex, there are several dramatic changes to the conformation of P-LE associated with binding of SGP-3 (Figures 6A and 6C). The most significant of these in terms of promoting direct binding contacts to SGP-3 is the translocation of the Asn83 to Asp89 loop in P-LE from the periphery to a position near the SLe^X binding site. This affords the hydrogen bond interactions mediated by Arg85 (see above) and brings Asn83 and Glu88 to positions where they simultaneously ligate the bound metal and form hydrogen bonds to Fuc (Figure 6C). The metal ligation by Glu88 now mimics that of MBP (corresponding residue is Glu193), unbound and complexed with oligomannose (Weis et al., 1992; Weis et al., 1991), a feature previously noted as distinguishing this lectin from the earlier E-LE structure (Graves et al., 1994). A loop of residues from Arg54 to Glu74 is displaced relative to the uncomplexed P-LE and P-LE/SLe^X structures and partially occupies the space vacated by the Asn83 to Asp89 loop (Figure 6A). Differences in P-LE conformation are also readily apparent at the interface of the two domains resulting in a 52° change in orientation of the EGF domain relative to the lectin domain (Figure 6A). In unliganded P-LE and the P-LE/SLe^X complex, Thr65 packs against the side chain of Trp1 excluding it from solvent. The movement of loops observed for the P-LE/SGP-3 complex would be expected to expose Trp1 to solvent, but this residue rearranges to pack between Tyr118 of the lectin domain and Glu135 of the EGF domain. A molecule of 2-methyl-2,4-pentanediol (MPD) used for crystallization fills the void created by the movement of the Trp1 side chain molecule (Figure 6A).

Although possibly an artifact of the crystallization conditions, the change in the conformation at the lectin-EGF domain interface is interesting in light of reports that the EGF domain may modulate selectin function (Kansas, 1996). As noted for the earlier E-LE crystal structure (Graves et al., 1994), the lectin domain makes a limited number of contacts with EGF residues 135–139; this is a property shared with all of our structures including the P-LE/SGP-3 complex. The small number of interactions between the lectin and EGF domains argues that this interface is inherently flexible. Of the three selectins, P-selectin may be the most flexible in this region

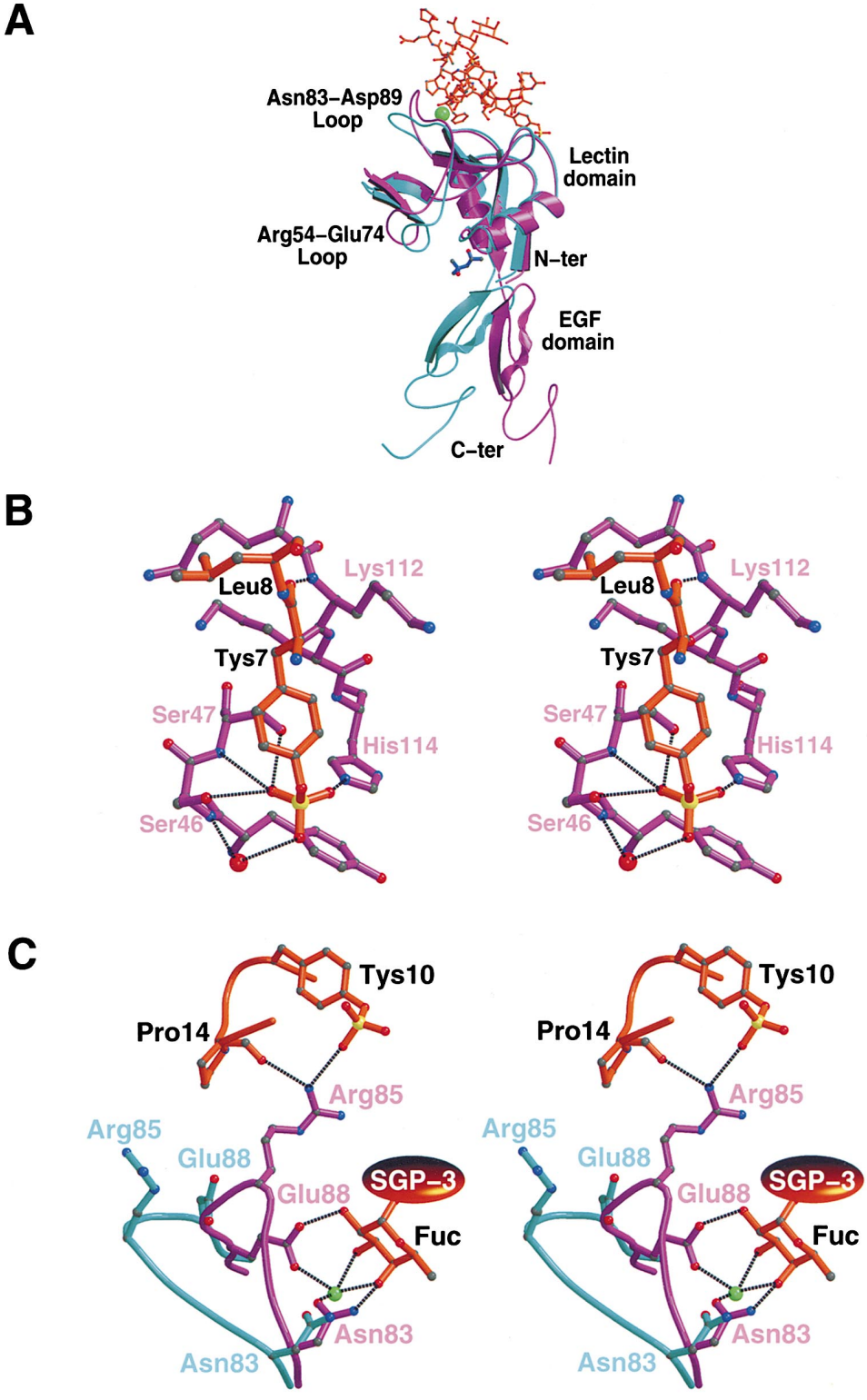

Figure 6. Structure of the P-LE/SGP-3 Complex and Binding Interactions Involving Tys Residues

(A) Ribbon/stick representation of the P-LE/SGP-3 structure superimposed on the unliganded structure of P-LE. The unliganded structure of P-LE is shown in blue, complexed P-LE in purple, and SGP-3 in orange. The bound strontium ion in the P-LE/SGP-3 complex is directly superimposed over the calcium ion in unliganded P-LE and is shown as a green sphere. The MPD molecule that is found at the lectin-EGF domain interface in the P-LE/SGP-3 complex is shown in dark blue.

(B) Stereo view of a close-up of P-LE/SGP-3 interactions in the region of Tys7 (in orange) illustrating the hydrogen bonding network with P-LE (purple). The sulfur atom in Tys7 is shown in yellow.

(C) Stereo view of a close-up of the P-LE/SGP-3 interaction in the region of Tys10 and the Fuc binding site illustrating the change in conformation and binding contacts for the Asn83 to Asp89 loop within P-LE. Uncomplexed P-LE is shown in blue and P-LE complexed with SGP-3 is shown in purple. SGP-3 residues are shown in orange (the sulfur atom of Tys10 is in yellow) and the bound strontium ion is shown as a green sphere. The portion of SGP-3 omitted for clarity is shown as an orange ellipse.

due to substitution of Gly138 for Asn138. Asn138 is conserved in human E- and L-selectin EGF domains and, in both E-LE crystal structures, forms stabilizing hydrogen bonds to the lectin domain via two water molecules. In contrast, Gly138 in P-selectin is unable to form these hydrogen bonds. Therefore, the P-selectin EGF domain may place fewer restrictions on the movement of the lectin domain. The freedom of motion of the lectin domain may be essential for maximizing contacts between P-selectin and PSGL-1 on free-flowing leukocytes.

Our models suggest that P-selectin exists in two conformations: a low-affinity form that supports SLe^X binding and a high-affinity form that is capable of making extended contacts with PSGL-1. It is possible that SLe^X binding alone also induces a conformational change in P-selectin, but this may be restricted by steric contacts in the preformed P-LE crystals. We see no evidence of even minor structural rearrangements, however, in any copy of SLe^X-bound P-LE within the crystal. Moreover, only minor improvements in SLe^X binding appear to be associated with this conformational change. Conversion of the unliganded or SLe^X-bound form of P-selectin to the high-affinity form may occur by one of two possible mechanisms. Interactions with PSGL-1 may initiate at the P-selectin binding site shown here; this induces conformational changes down one face of the lectin domain that are ultimately transmitted to the lectin-EGF domain interface. Alternatively, mechanical perturbation of the lectin-EGF domain interface (e.g., by nonspecific contact with circulating cells) may activate P-selectin to the high-affinity form by triggering conformational changes that move up the face of the lectin domain toward the PSGL-1 binding site. Additional studies are required to further explore these possibilities.

Concluding Remarks

We find that a common element in E- and P-selectin bound to SLe^X and P-selectin complexed with PSGL-1 is an intricate network of relatively few but optimally disposed interactions that are largely electrostatic in nature. This is consistent with the rapid binding kinetics described for this family of adhesion receptors. Our results offer a structural basis for affinity differences between E- and P-selectin for this ligand and counterreceptor that likely reflects specialized roles in the recruitment of leukocytes to sites of inflammation. In particular, the structure of the P-LE/SGP-3 complex reveals molecular contacts that likely distinguish PSGL-1 interactions with P-selectin from those with E-selectin. In human P-selectin, amino acid residues Arg85 and His114 provide critical contacts to the sulfates on Tyr7 and Tyr10 of PSGL-1. In contrast, these interactions are presumably not formed in human E-selectin in which the corresponding residues are Gln85 and Leu114. It is noteworthy that between different mammalian species there is an evolutionary conservation of this feature; similar differences in charge also occur at these positions in the mouse, rat, rabbit, and cow homologues of P-selectin and E-selectin.

Our results also provide insights into the nature of L-selectin interactions with PSGL-1 in the context of inflammation, as well as with sulfated SLe^X-type glycans important for lymphocyte homing. L-selectin may bind PSGL-1 in a similar fashion to P-selectin based on the conservation of residues within the SLe^X binding site and a basic residue (Lys) at position 85. We have observed that a LE construct of L-selectin binds to SGP-3 with weaker affinity ($K_D = 40\ \mu M$, data not shown) than that of P-LE. The P-LE/SGP-3 structure predicts this lower affinity interaction, as L-selectin lacks the basic residue at position 114 needed to interact with the second tyrosine sulfate within PSGL-1. L-selectin binds weakly to SLe^X but with improved affinity to SLe^X modified by sulfate at the 6-hydroxyl positions of Gal and/or GlcNAc (Bistrup et al., 1999) displayed by one or more glycoprotein counterreceptors in HEV of secondary lymphoid organs (Kansas, 1996). The shared requirement of sulfate for recognition of these glycans and PSGL-1 raises the possibility of a common L-selectin binding motif for this posttranslational modification. Simple modeling of sulfate groups onto SLe^X within our complexes indicates that these do not directly superimpose with tyrosine sulfates within the SGP-3 structure. Therefore, the orientation of sulfated SLe^X within the L-selectin binding site or the conformation of the lectin domain may differ subtly from the structures presented here. Elucidation of the binding interactions with sulfated SLe^X as well as those with PSGL-1 awaits the structure determination of L-selectin complexed with this ligand and counterreceptor.

Experimental Procedures

Generation of Constructs and Protein/Peptide Preparation

Constructs encoding the lectin-EGF (LE) domains of human P- and E-selectin fused to the CH2-CH3 region of human IgG_1 via an intervening enterokinase (EK) cleavage sequence (Asp-Asp-Asp-Asp-Lys) were expressed in CHO cells and recovered from conditioned media by protein A sepharose (Pharmacia) chromatography. Monomeric selectin LE domains were produced by digestion of the dimeric Fc constructs with EK (LaVallie et al., 1993). The selectin LE domains were deglycosylated at 37° C for 48 hr at a ratio of 25 milliunits N-glycanase/mg protein and purified by anion exchange and hydrophobic interaction chromatography. P-LE and E-LE were determined to be correct by MS, monomeric by gel filtration HPLC, and functional by surface plasmon resonance (BIAcore) analyses. The liberated LE-domains correspond to the N-terminal 157 amino acids of the mature proteins beginning at conserved residue Trp1. Both constructs contain the five residue C-terminal EK sequence.

The expression in CHO cells of a soluble, enterokinase-sensitive Fc construct of human PSGL-1 (19ek.Fc) was described earlier (Goetz et al., 1997). 19ek.Fc was digested with EK and the liberated, heterogenous 19ek peptides were purified to individual species. Amino acid and carbohydrate composition analyses, NMR spectroscopy, and MALDI-TOF and ESI MS (in the negative ion modes) before and after proteolytic and glycosidic digestions were used to determine the 19ek peptide structures (J. Rouse, D. Tsao, and R. T. C., unpublished data).

P-LE/19ek Peptide Binding Studies

Surface plasmon resonance was performed on BIAcore 2000 and 3000 instruments at 25° C using streptavidin-coated sensor chips (BIAcore) and HBS-P buffer (BIAcore; 10 mM HEPES [pH 7.4], 150 mM NaCl, and 0.005% polysorbate 20 [v/v]) adjusted to 1 mM each $CaCl_2$ and $MgCl_2$. The 19ek peptides and sPSGL, a construct consisting of the entire dimeric, extracellular domain of PSGL-1 (Croce et al., 1998), were biotinylated at Lys residues with Sulfo-NHS-LC-Biotin (Pierce). Following biotinylation, sPSGL was reacted with immobilized P-selectin in order to isolate functional material (Sako et

al., 1995). A synthetic peptide (AnaSpec, Inc.) corresponding to the polypeptide portion of SGP-3 was similarly biotinylated. Biotinylated PSGL-1 constructs were coated onto sensor chips using HBS-P buffer. Glycosylated P-LE was injected over the 19ek peptide, sPSGL and control surfaces at 40 μL/min. The specificity of binding was validated by control experiments performed in the presence of neutralizing Mab to P-selectin, 10 mM EDTA, and soluble 19ek peptides (R. Camphausen, unpublished data). Deglycosylated P-LE bound comparably to the glycosylated version.

Crystallization and Data Collection

All diffraction data were collected in-house on Rigaku RU200 generators running at 5.0 KW with Yale/Molecular Structure Corp. focusing mirrors and on RAXIS II or RAXIS IV image plate area detectors except where noted.

Crystals of P-LE were grown at 18°C using vapor diffusion from a solution containing 10 mg/ml protein, 100 mM Tris-HCl (pH 8.5), 150 mM NaCl, 12 mM $CaCl_2$, 10% (v/v) 2-methyl-2,4-pentanediol (MPD), and 10% (w/v) PEG 6000. These crystals were transferred into 100 mM Tris-HCl (pH 8.5), 75 mM NaCl, 10 mM $CaCl_2$, 10% (v/v) MPD, and 11% (w/v) PEG 6000, then transferred for two hours to the same buffer diluted by 5% (v/v) with MPD. After a second 5% dilution with MPD the crystal was soaked for 13 hr prior to flash cooling in liquid propane held at liquid nitrogen temperature. P-LE complexed with SLe^X (SLe^X-β-O-methyl, Toronto Research Chemicals) was obtained using the same methods but with the addition of 8 mM SLe^X to the final soaking solution. The space group of the P-LE crystals was $P2_1$ with cell parameters a = 81.0 Å, b = 60.8 Å, c = 91.4 Å, and β=103.6°. Soaking crystals in SLe^X reduced the maximum resolution to 3.4 Å, increased the mosaicity to 1.5° and gave cell parameters a = 81.1 Å, b = 60.5 Å, c = 91.4 Å and β = 103.3°. Diffraction data were processed and scaled with DENZO/SCALEPACK (HRL Research, Inc.) giving the statistics reported in Table 1.

Crystals of E-LE were obtained using vapor diffusion at 18°C from a solution containing 30 mg/ml protein, 100 mM HEPES (pH 7.5), 10 mM Tris-HCl, 200 mM $CaCl_2$, and 15% (w/v) PEG 4000. For complexes with SLe^X, E-LE crystals were transferred to a solution containing 100 mM HEPES (pH 7.5), 200 mM $CaCl_2$, 30% (w/v) PEG 4000, and 15 mM SLe^X for 15 hr at 25°C. After this initial incubation, crystals were transferred into 100 mM Tris-HCl (pH 7.4), 300 mM NaCl, 2 mM $CaCl_2$, 30% (w/v) PEG 4000, and 15 mM SLe^X for an additional hour prior to flash cooling as described above. The E-LE/SLe^X crystals belonged to space group $P2_12_12_1$ with cell parameters a = 34.5 Å, b = 72.4 Å, and c = 77.6 Å. Diffraction data were processed as above.

Crystals of the P-LE/PSGL-1 19ek peptide (SGP-3) complex were obtained from 8 mg/ml P-LE, SGP-3 in a 2-fold molar excess, 100 mM HEPES (pH 7.0), 10 mM Tris-HCl, 150 mM NaCl, 4 mM $CaCl_2$, 50 mM $SrCl_2$, 5% (w/v) PEG 6000, and 33% (v/v) MPD. Crystals were transferred into 100 mM HEPES (pH 7.0), 10% PEG 6000, 30% MPD, 100 mM NaCl, and 50 mM $SrCl_2$ for 15 hr prior to flash cooling. A mercury-derivatized crystal was obtained by adding 0.5 mM mercury acetate to the final soaking buffer. The space group of the complex crystals was found to be I222 with cell parameters a = 63.4 Å, b = 96.8 Å, and c = 187.3 Å. Native diffraction data were collected at beamline X4A at the National Synchrotron Light Source (NSLS) at Brookhaven National Laboratory using a wavelength of 0.99987 Å. The mercury derivative data were collected in-house. All data were reduced as described above giving statistics in Table 1.

Structure Determination and Refinement

Crystals of E-LE complexed with SLe^X were found to be essentially isomorphous with those of the previously described E-LE construct (Graves et al., 1994) with a single copy of E-LE in the crystallographic asymmetric unit. Rigid body refinement within CNS (Brunger et al., 1998) was used to obtain initial phases that gave clear electron density for the bound SLe^X. These maps were further improved with the use of BUSTER (Bricogne, 1993), allowing a model for bound SLe^X to be fitted using QUANTA (Molecular Simulations, Inc.). All further refinement was performed in CNS, giving a final model with 86% of residues in the most favored region of the Ramachandran plot and consisting of a total of 1510 atoms, 186 water molecules, one calcium ion, and one copy of SLe^X. The model contains E-LE residues 1–157. Residues associated with the EK sequence were not observed. Statistics are described in Table 1.

The structure of P-LE was solved with molecular replacement using the published model of the E-lec/EGF construct (PDB accession code 1ESL). The program AMORE (CCP4, 1994) was used to locate all four copies of P-LE. The model was built and refined using the methods described above giving the statistics in Table 1. The final model consists of four copies of P-LE with 81% of the residues in the most favored regions of the Ramachandran plot, 5418 total atoms, 134 water molecules, two MPD molecules, and four calcium ions. All four copies contain residues 1–157 of the P-selectin sequence and the first Asp residue of the EK sequence. Additional residues in the EK sequence (one or two) are modeled as alanine.

The crystals of P-LE soaked in SLe^X were essentially isomorphous with the P-LE structure described above. After rigid body refinement in CNS, there was clear density for three bound SLe^X molecules. The fourth binding site was partially occluded by crystal contacts, thus explaining the loss of resolution upon soaking in SLe^X. QUANTA was used to model bound SLe^X and refit protein residues before limited refinement in CNS. This gave a final model consisting of four copies of P-LE (residue content is identical to unliganded forms above) with 71% of the residues in the most favored Ramachandran regions, 5455 total atoms, three SLe^X molecules, four calcium ions and two MPD molecules. The four copies contain the P-selectin sequence and portions of the EK sequence as in the above.

All attempts to solve the structure of P-LE complexed with the PSGL-1 19ek peptide SGP-3 by molecular replacement failed. The heavy atom site was located with Patterson techniques refined in SHARP (de la Fourtelle and Bricogne, 1997). These phases gave poor maps but of sufficient quality to allow positioning of two lectin domains from the P-LE structure and independent positioning of two EGF domains. These maps also indicated the presence of bound SLe^X molecules in the same position as found in the P-LE/SLe^X complex and extra density that could not be interpreted. The heavy atom phases were combined with model phases in BUSTER giving clear maximum entropy maps that allowed fitting of the SGP-3 polypeptide and SLe^X moieties in QUANTA. This structure was refined as described above giving statistics in Table 1 and 84% of residues in the most favored regions of the Ramachandran plot. The final model consists of two P-LE/SGP-3 complexes, 3263 atoms, two strontium ions, 224 water molecules, two sodium ions, and seven bound MPD molecules. One copy of the P-LE/SGP-3 complex contains P-LE residues 1–157 and one residue of the EK sequence modeled as alanine; the other contains P-LE residues 1–156 and residue 157 modeled as alanine. Both copies contain SGP-3 residues as described in Results and Discussion.

Acknowledgments

We thank Monique Davies and Kenneth Comess for the development of the 19ek.Fc cell line, Richard Zollner and his colleagues for the generation of large quantities of conditioned media, Mark Stahl and Holly Schmidt for purification assistance, Jason Rouse and Desiree Tsao for assistance with the characterization of the 19ek peptides, Craig Ogata of the NSLS at Brookhaven National Laboratory for assistance with crystallographic data collection, and David Erbe for critical reading of the manuscript. We also wish to acknowledge John Knopf and Jasbir Seehra for their support.

Received May 23, 2000; revised September 7, 2000.

References

Alon, R., Chen, S., Puri, K.D., Finger, E.B., and Springer, T.A. (1997). The kinetics of L-selectin tethers and the mechanics of selectin-mediated rolling. J. Cell Biol. *138*, 1169–1180.

Alon, R., Hammer, D.A., and Springer, T.A. (1995). Lifetime of the P-selectin-carbohydrate bond and its response to tensile force in hydrodynamic flow. Nature *374*, 539–542.

Asa, D., Gant, T., Oda, Y., and Brandley, B.K. (1992). Evidence for two classes of carbohydrate binding sites on selectins. Glycobiology *2*, 395–399.

Bajorath, J., Hollenbaugh, D., King, G., Harte, W., Eustice, D.C., Darveau, R.P., and Aruffo, A. (1994). CD62/P-selectin binding sites for myeloid cells and sulfatides are overlapping. Biochemistry *33*, 1332–1339.

Bertozzi, C.R. (1995). Cracking the carbohydrate code for selectin recognition. Chem. Biol. *2*, 703–708.

Bistrup, A., Bhakta, S., Lee, J.K., Belov, Y.Y., Gunn, M.D., Zuo, F.R., Huang, C.C., Kannagi, R., Rosen, S.D., and Hemmerich, S. (1999). Sulfotransferases of two specificities function in the reconstitution of high endothelial cell ligands for L-selectin. J. Cell Biol. *145*, 899–910.

Bricogne, G. (1993). Direct phase determination by entropy maximization and likelihood ranking; status report and perspectives. Acta Crystallogr. *D49*, 37–60.

Brunger, A.T., Adams, P.D., Clore, G.M., DeLano, W.L., Gros, P., Grosse-Kunstleve, R.W., Jiang, J.S., Kuszewski, J., Nilges, M., Pannu, N.S., et al. (1998). Crystallography and NMR system: a new software suite for macromolecular structure determination. Acta Crystallogr. *D54*, 905–921.

CCP4 (1994). The CCP-4 suite: programs for X-ray crystallography. Acta Crystallogr. *D50*, 760–763.

Chen, S., Alon, R., Fuhlbrigge, R.C., and Springer, T.A. (1997). Rolling and transient tethering of leukocytes on antibodies reveal specializations of selectins. Proc. Natl. Acad. Sci. USA *94*, 3172–3177.

Croce, K., Freedman, S.J., Furie, B.C., and Furie, B. (1998). Interaction between soluble P-selectin and soluble P-selectin glycoprotein ligand 1: equilibrium binding analysis. Biochemistry *37*, 16472–16480.

de la Fourtelle, E., and Bricogne, G. (1997). Maximum-likelihood heavy-atom parameter refinement for multiple isomorphous replacement and multiwavelength anomalous diffraction methods. Methods Enzymol. *276*, 472–494.

Drickamer, K. (1988). Two distinct classes of carbohydrate-recognition domains in animal lectins. J. Biol. Chem. *263*, 9557–9560.

Epperson, T.K., Patel, K.D., McEver, R.P., and Cummings, R.D. (2000). Noncovalent association of P-selectin glycoprotein ligand-1 and minimal determinants for binding to P-selectin. J. Biol. Chem. *275*, 7839–7853.

Foxall, C., Watson, S.R., Dowbenko, D., Fennie, C., Lasky, L.A., Kiso, M., Hasegawa, A., Asa, D., and Brandley, B.K. (1992). The three members of the selectin receptor family recognize a common carbohydrate epitope, the sialyl Lewis X oligosaccharide. J. Cell Biol. *117*, 895–902.

Goetz, D.J., Greif, D.M., Ding, H., Camphausen, R.T., Howes, S., Comess, K.M., Snapp, K.R., Kansas, G.S., and Luscinskas, F.W. (1997). Isolated P-selectin glycoprotein ligand-1 dynamic adhesion to P- and E-selectin. J. Cell Biol. *137*, 509–519.

Graves, B.J., Crowther, R.L., Chandran, C., Rumberger, J.M., Li, S., Huang, K.S., Presky, D.H., Familletti, P.C., Wolitzky, B.A., and Burns, D.K. (1994). Insight into E-selectin/ligand interaction from the crystal structure and mutagenesis of the lec/EGF domains. Nature *367*, 532–538.

Honig, B., and Nicholls, A. (1995). Classical electrostatics in biology and chemistry. Science *268*, 1144–1149.

Kansas, G.S. (1996). Selectins and their ligands: current concepts and controversies. Blood *88*, 3259–3287.

Kraulis, P.J. (1991). MOLSCRIPT: a program to produce both detailed and schematic plots of protein structures. J. Appl. Crystallogr. *24*, 946–950.

LaVallie, E.R., Rehemtulla, A., Racie, L.A., DiBlasio, E.A., Ferenz, C., Grant, K.L., Light, A., and McCoy, J.M. (1993). Cloning and functional expression of a cDNA encoding the catalytic subunit of bovine enterokinase. J. Biol. Chem. *268*, 23311–23317.

Leppanen, A., Mehta, P., Ouyang, Y.B., Ju, T., Helin, J., Moore, K.L., van Die, I., Canfield, W.M., McEver, R.P., and Cummings, R.D. (1999). A novel glycosulfopeptide binds to P-selectin and inhibits leukocyte adhesion to P-selectin. J. Biol. Chem. *274*, 24838–24848.

Li, F., Erickson, H.P., James, J.A., Moore, K.L., Cummings, R.D., and McEver, R.P. (1996). Visualization of P-selectin glycoprotein ligand-1 as a highly extended molecule and mapping of protein epitopes for monoclonal antibodies. J. Biol. Chem. *271*, 6342–6348.

McEver, R.P., and Cummings, R.D. (1997). Role of PSGL-1 binding to selectins in leukocyte recruitment. J. Clin. Invest. *100*, S97–103.

Mehta, P., Cummings, R.D., and McEver, R.P. (1998). Affinity and kinetic analysis of P-selectin binding to P-selectin glycoprotein ligand-1. J. Biol. Chem. *273*, 32506–32513.

Mehta, P., Patel, K.D., Laue, T.M., Erickson, H.P., and McEver, R.P. (1997). Soluble monomeric P-selectin containing only the lectin and epidermal growth factor domains binds to P-selectin glycoprotein ligand-1 on leukocytes. Blood *90*, 2381–2389.

Merrit, E.A., and Murphy, M.E.P. (1994). Raster3D version 2.0: a program for photorealistic molecular graphics. Acta Crystallogr. *D50*, 869–873.

Moore, K.L., Eaton, S.F., Lyons, D.E., Lichenstein, H.S., Cummings, R.D., and McEver, R.P. (1994). The P-selectin glycoprotein ligand from human neutrophils displays sialylated, fucosylated, O-linked poly-N-acetyllactosamine. J. Biol. Chem. *269*, 23318–23327.

Nicholls, A., Sharp, K., and Honig, B. (1991). Protein folding and association: insights from the interfacial and thermodynamic properties of hydrocarbons. Proteins *11*, 281–296.

Poppe, L., Brown, G.S., Philo, J.S., Nikrad, P.V., and Shah, B.H. (1997). Conformation of the sLe^x tetrasaccharide, free in solution and bound to E-, P-, and L-selectin. J. Am. Chem. Soc. *119*, 1727–1736.

Pouyani, T., and Seed, B. (1995). PSGL-1 recognition of P-selectin is controlled by a tyrosine sulfation consensus at the PSGL-1 amino terminus. Cell *83*, 333–343.

Puri, K.D., Chen, S., and Springer, T.A. (1998). Modifying the mechanical property and shear threshold of L-selectin adhesion independently of equilibrium properties. Nature *392*, 930–933.

Ramachandran, V., Nollert, M.U., Qiu, H., Liu, W.J., Cummings, R.D., Zhu, C., and McEver, R.P. (1999). Tyrosine replacement in P-selectin glycoprotein ligand-1 affects distinct kinetic and mechanical properties of bonds with P- and L- selectin. Proc. Natl. Acad. Sci. USA *96*, 13771–13776.

Sako, D., Chang, X.-J., Barone, K.M., Vachino, G., White, H.M., Shaw, G., Veldman, G.M., Bean, K.M., Ahern, T.J., Furie, B., et al. (1993). Expression cloning of a functional glycoprotein ligand for P-selectin. Cell *75*, 1179–1186.

Sako, D., Comess, K.M., Barone, K.M., Camphausen, R.T., Cumming, D.A., and Shaw, G.D. (1995). A sulfated peptide segment at the amino terminus of PSGL-1 is critical for P-selectin binding. Cell *83*, 323–331.

Skrzypczak-Jankun, E., Carperos, V.E., Ravichandran, K.G., Tulinsky, A., Westbrook, M., and Maraganore, J.M. (1991). Structure of the hirugen and hirulog 1 complexes of alpha-thrombin. J. Mol. Biol. *221*, 1379–1393.

Springer, T.A. (1994). Traffic signals for lymphocyte recirculation and leukocyte emigration: the multistep paradigm. Cell *76*, 301–314.

Varki, A. (1994). Selectin ligands. Proc. Natl. Acad. Sci. USA *91*, 7390–7397.

Varki, A. (1997). Selectin ligands: will the real ones please stand up? J. Clin. Invest. *100*, S31–35.

Vestweber, D., and Blanks, J.E. (1999). Mechanisms that regulate the function of the selectins and their ligands. Physiol. Rev. *79*, 181–213.

Weis, W.I., Drickamer, K., and Hendrickson, W.A. (1992). Structure of a C-type mannose-binding protein complexed with an oligosaccharide. Nature *360*, 127–134.

Weis, W.I., Kahn, R., Fourme, R., Drickamer, K., and Hendrickson, W.A. (1991). Structure of the calcium-dependent lectin domain from a rat mannose-binding protein determined by MAD phasing. Science *254*, 1608–1615.

Wilkins, P.P., McEver, R.P., and Cummings, R.D. (1996). Structures of the O-glycans on P-selectin glycoprotein ligand-1 from HL-60 cells. J. Biol. Chem. *271*, 18732–18742.

Wilkins, P.P., Moore, K.L., McEver, R.P., and Cummings, R.D. (1995). Tyrosine sulfation of P-selectin glycoprotein ligand-1 is required for high affinity binding to P-selectin. J. Biol. Chem. *270*, 22677–22680.

Yang, J., Furie, B.C., and Furie, B. (1999a). The biology of P-selectin glycoprotein ligand-1: its role as a selectin counterreceptor in leukocyte-endothelial and leukocyte-platelet interaction. Thromb. Haemost. *81*, 1–7.

Yang, J., Hirata, T., Croce, K., Merrill-Skoloff, G., Tchernychev, B., Williams, E., Flaumenhaft, R., Furie, B.C., and Furie, B. (1999b). Targeted gene disruption demonstrates that P-selectin glycoprotein ligand 1 (PSGL-1) is required for P-selectin-mediated but not E-selectin-mediated neutrophil rolling and migration. J. Exp. Med. *190*, 1769–1782.

Protein Data Bank ID Codes

Coordinates have been deposited in the Protein Data Bank under ID codes 1G1Q for P-LE, 1G1R for P-LE/SLe^x, 1G1T for E-LE/SLe^x, and 1G1S for P-LE/SGP-3.